Int. J. Electrochem. Sci., 13 **(2018)** 12049 – 12061, doi: 10.20964/2018.12.18

International Journal of
ELECTROCHEMICAL
SCIENCE
www.electrochemsci.org

Pyrolytic carbon felt electrode Inhibits Formation of Zinc Dendrites in Zinc Bromine Flow Batteries

Hang Lin[1,*], *Lufei Bai*[1], *Xu Han*[1], *Yu Zhang*[1], *Junyou Shi*[1,2,*]

[1] Department of Chemical Engineering, Northeast Electric Power University, Jilin 132012, China.
[2] Department of Forestry, Beihua University, Jilin 132012, China.
[*]E-mail: hilinhang@sina.com, bhsjy64@163.com.

Received: 24 July 2018 / *Accepted:* 16 September 2018 / *Published:* 5 November 2018

Zinc bromine flow batteries (ZBFBs) can provide energy storage with a high energy density and good efficiency, at moderate costs. However, faster technical development at a large scale have restricted faster development. In particular, in the charging process, uneven deposition of zinc easily forms zinc dendrites and pierces the separator to cause serious self-discharge of the battery, which greatly reduces the coulombic efficiency and service life. Pyrolytic method can improve the electrochemical properties of the carbon felt (CF) and effectively promote the uniform deposition of zinc in the ZBFBs. In this work, we found that the zinc deposits formed on the CF surface after calcined at 500 °C are tight and uniform, and the deposition quality is much better than that of the untreated ones. In terms of performance, compared with the original CF as the negative electrode of the zinc-bromine battery, operating at a current density of 40 mA cm^{-2}, the coulombic efficiency increased from 91.8% to 99.3%, and the energy efficiency increased from 71.8% to 81.9%. Even at a current density of 80 mA cm^{-2}, the energy efficiency is as high as 69.8%.

Keywords: Uniform deposition, Zinc dendrites, Pyrolytic carbon, Carbon felt.

1. INTRODUCTION

With the continuous depletion of fossil energy, people are increasingly drawing up and utilizing renewable energy such as wind energy, hydropower, and solar energy [1]. However, renewable energy sources are volatile and unstable, which can cause a huge impact on the power grid. Therefore, energy storage technology is needed to splice intermittent renewable energy sources [2-3], improve the stability of the power system, encourage the development of renewable energy sources, and increase the utilization and stability of the power grid [4]. In recent years, the redox flow battery has been the most promising candidate for large-scale energy storage technology [5-6], due to its modular design, low cost, and high efficiency. To date, various flow battery systems have been

proposed and developed, including all-vanadium [7-9], Fe/Cr [10-12], sodium polysulfide/Br_2 [13], and Zn/Br_2 [14-16].

Among them, zinc bromide flow batteries (ZBFBs) have the highest theoretical specific energy, up to 440 W h kg^{-1} at 298 K [17], and the most widely studied vanadium-based flow batteries have only 35 W h kg^{-1} of specific energy [18], which means that the same stack size can be stored more energy, coupled with relatively low cost, high energy efficiency, should have been the most promising large-scale energy storage technology, but its technical problems have been restricting its further development. During the charging process, due to the uneven deposition of zinc on the negative electrode, zinc dendrites are easily formed [17]. With the continuous growth of the dendrites, the separator would be broken and the positive and negative electrolytes would be mixed, resulting in a profound self-discharge phenomenon. Even when the dendrite contacts the counter electrode through the membrane, it causes an internal short circuit of the battery, degrading battery performance and service life, which is part of the major technical issues of ZBFBs. Unlike full-flow systems (such as all-vanadium redox flow batteries), the active material is always dissolved in the electrolyte and the energy can be uncoupled from the power, But ZBFBs are actually a hybrid flow system, during the charging process, zinc is deposited on the negative electrode, so its energy depends on the size of the battery pack and is coupled with power [19]. That is, at a given stack size, the discharge capacity of the ZBFBs depends on the amount and quality of zinc loading on the electrode surface, and the electrodes are not involved in the charge-discharge reaction. Not only that, the dendrite and the electrode are not firmly bonded and are easily detached from the electrode surface, resulting in energy loss discharge voltage fluctuation. Unfortunately, until now, bromine side reactions have received more attention, but zinc side reactions have rarely been noticed. Electrochemical reactions of ZBFBs positive and negative electrodes are as follows:

$$\text{Negative: } Zn^{2+} + 2e \Leftrightarrow Zn \quad E_0 = -0.76\ \text{V}\ vs.\ \text{SHE} \quad (1)$$

$$\text{Positive: } 2Br^- - 2e \Leftrightarrow Br_2 \quad E_0 = +1.07\ \text{V}\ vs.\ \text{SHE} \quad (2)$$

$$\text{Overall: } \text{ZnBr}_2 \Leftrightarrow Zn + Br_2 \quad E_0 = +1.83\ \text{V}\ vs.\ \text{SHE} \quad (3)$$

So far, the mechanism of zinc dendrite formation is not evident. It is generally accepted to be caused by uneven distribution of exchange current density in various regions of the electrode surface caused by electrode polarization [20-21], and is mainly affected by applied current density and overpotential [22]. Carbon felt (CF) is made of carbon fiber and has an amorphous carbon structure [23], which is the preferred electrode material for some redox flow batteries due to its advantages of low cost, large porosity, high temperature resistance and good chemical stability [24-26], and it is also the main electrode material for ZBFBs [27]. However, low electrochemical activity and hydrophilicity cannot fully satisfy the requirements of ZBFBs electrodes. High temperature graphitization is a convenient and efficient modification method and can improves the electrochemical activity and electrical conductivity of the CFs [28-31], however, during the high temperature graphitization process, the impurity element escapes from the CF, and the carbon on the surface of the CF is evaporated, thereby forming various defects, which in turn enlarges the polarization of the electrode. Therefore, we proposed a pyrolytic method to modify CF electrodes. In this way, methane gas can be in addition to the inert gas. Under high temperature heating, methane will be cracked, and the formed

carbon will deposit at the defects of the carbon fiber, which will fill the defects caused by the sublimation of the carbon fiber at high temperature. After this series of processed CFs are transformed from disordered structures to order structures, and the depolarization ability of the CF electrodes are enhanced, and the uniform deposition of zinc can be promoted. Carburizing technology can be used in the high-temperature heat treatment process to fill the defects of carbon fiber, thereby improving the degree of graphitization and surface smoothness of CF and in turn catalyzes the redox reaction, increasing the efficiency of the battery.

In our work, we prepared a pyrolytic carbon felt by controlling the temperature, and obtained the optimum temperature conditions for the preparation of the modified carbon felt electrode. The electrochemical performance of CFs were measured by CV and EIS, and the results showed that the deposition performance of CF-500 °C was the best. The CF-500 °C electrode was assembled into a battery for constant current charge and discharge and compared with the original carbon felt electrode. We found that the zinc deposited on the CF-500 °C electrode was more uniform and had no dendrite formation, and the battery performance with CF-500 °C electrode was superior to that of the original CF electrode.

2. EXPERIMENTAL SECTION

2.1. Thermal modification of CFs

Commercial carbon felt (Tianjin Carbon Co., Ltd.) with a thickness of 3 mm was ultrasonically cleaned with acetone, ethanol, and deionized water for 10 minutes, respectively, and dried overnight in a vacuum drying oven. The pretreated CF was placed in a tube furnace and calcined at 350 °C, 400 °C, 450 °C, 500 °C and 550 °C with the heating rate of 5 °C min^{-1} for 5 h under flowing mixed gas of Ar and methane (50 mL min-1, 2 MPa) to fabricate the pyrolytic carbon felt electrode electrodes.

2.2. Three-electrode test

Cyclic voltammetry (CV) and electrochemical impedance spectroscopy (EIS) measurements were performed using an electrochemistry station (CHI660E). The pyrolytic CFs and the untreated CF electrode were cut into 10 mm × 10 mm active area as a working electrodes. The auxiliary electrode is a platinum electrode, and the reference electrode is a saturated calomel electrode (SCE), which was verified in an electrolyte of 0.05 M $ZnBr_2$ + 0.05 M KCl. CV initial scan potential is 0 V, and the potential scan window is from 0 V to -1.1 V (vs. SCE) at a scan rate of 10 mv s^{-1}. EIS was performed by applying a 10 mV magnitude in the frequency range of 10 to 10^5 Hz. The potential is at the rate of deposition potentials to ensure zinc deposition.

2.3. Characterization of CF electrodes

The surface morphology of the pyrolytic CF electrodes and the zinc deposition morphology were observed by a scanning electron microscope (JMS-6480A) at an accelerating voltage of 15.0 kV. The X-ray diffraction (XRD) pattern was obtained from an XRD system (XRD-7000) with a scan angle of 10-90°and a scan rate of 5° min^{-1}. The Raman spectra of the original CF and the pyrolytic CF were obtained from the Raman system (LabRam-1B) at an excitation wavelength of 532 nm.

2.4. ZBFBs assembly and test

A laboratory-scale ZBFB was assembled for battery testing. The original CF was used as a positive electrode, and the original and pyrolytic CF was used as a negative electrode for comparison, which was cut into 20 mm × 20 mm and separated by Nafion 115 (DuPont, USA) membrane. 2 mm void space was reserved on the negative side for zinc deposition. 100 mL positive and negative electrolytes consist of 2 M $ZnBr_2$+2 M KCl and flowed through the dual-channel flow pump to the positive and negative electrodes with a fixed flow rate of 46 mL min^{-1}. The assembled ZBFB used a battery test system (BTS 9000) for galvanization charge and discharge and cycle of charge and discharge. The current density of the galvanization charge and discharge was from 20 to 80 mA cm^{-2}, the battery was charged for 30 min, and then discharged to a cut-off voltage of 0.5 V. Cycling performance was performed at 40 mA cm^{-2} for 50 cycles.

3. RESULTS AND DISCUSSION

A typical CV of zinc deposition on CF is shown in Fig. 1a. The scan is initiated at E_0 = 0 V, and then during the scan in the negative direction, once the zinc deposition is formed, the cathode current sharply increased, the corresponding potential is the deposition potential (DP). In the reverse scan, a current loop is formed due to the hysteresis of the potential. This observation of current crossover, the appearance of a hysteresis loop is characteristic of zinc nucleation and growth processes [32]. The potential at the cross point of the current loop is the crossover potential (COP), which coincides with the equilibrium potential of the Zn^{2+}/Zn couple. The difference between the COP and the DP is called the deposition overpotential (NOP). The smaller the NOP, the sharper the current loop, the more uniform the zinc deposition, and the better the deposition quality [33].

Fig. 1b shows the comparison of cyclic voltammetry between original CFs and pyrolytic CFs at different temperatures. We found that the DPs of the pyrolytic CF is smaller and the deposition currents was larger at E= -1.1 V than that of the untreated one, indicating that the kinetics of the Zn^{2+}/Zn on the treated CFs surface as well as the wettability are greatly improved. Moreover, as the processing temperature increased, DPs gradually decreased and the deposition current at E= -1.1 V increased, reaching an extremum at 500 °C, suggesting that the performance of Zinc deposition is best promoted by CF calcined at 500 °C. However, CF calcined at 550 °C, the DP is increased and the cathodic current is sharply reduced, which may be due to the fact that the temperature is too high, the

etching reactions of the surface carbon fibers are intensified, and the carbon fibers are obviously damaged and the deterioration of the zinc deposition kinetics[34]. From Tab 1, the CF-500 °C has the smallest NOP value of 59 mV. From the electrochemical point of view, the Zn deposition at CF-500 °C is the most uniform and the best quality [33]. During retrace, an oxidation peak appeared, corresponding to the process of re-oxidation of the deposited zinc. That is a de-galvanizing process that can eliminates protruding zinc deposits and effectively remove zinc dendrites. The greater the oxidation peak current, the better the deposition zinc dissolution reaction, which is consistent with the results of the deposition current. CF-500 °C has the largest oxidation peak current and exhibits excellent de-zincification performance. However, the oxidation peak of the CF treated at 550 °C is significantly negatively shifted, suggesting that excessive high-temperature oxidation of the CF surface may degrade the kinetics of the deposited zinc dissolution. Thus, these results show that mild oxidation of the CF at 500 °C is enough to boost the electrochemical activity for Zn^{2+}/Zn redox reactions. In order to test the stability of CF-500 °C electrodes in ZBFBs, CV results of 50 cycles were recorded at a scan rate of 10 mV s^{-1} and are given in Fig. 1c. It can be seen that the CV curve of the CF-500 °C electrode obtained at the 50th cycle is almost the same as the first cycle, which means that the CF-500 °C shows good stability and high durability in the ZBFBs system.

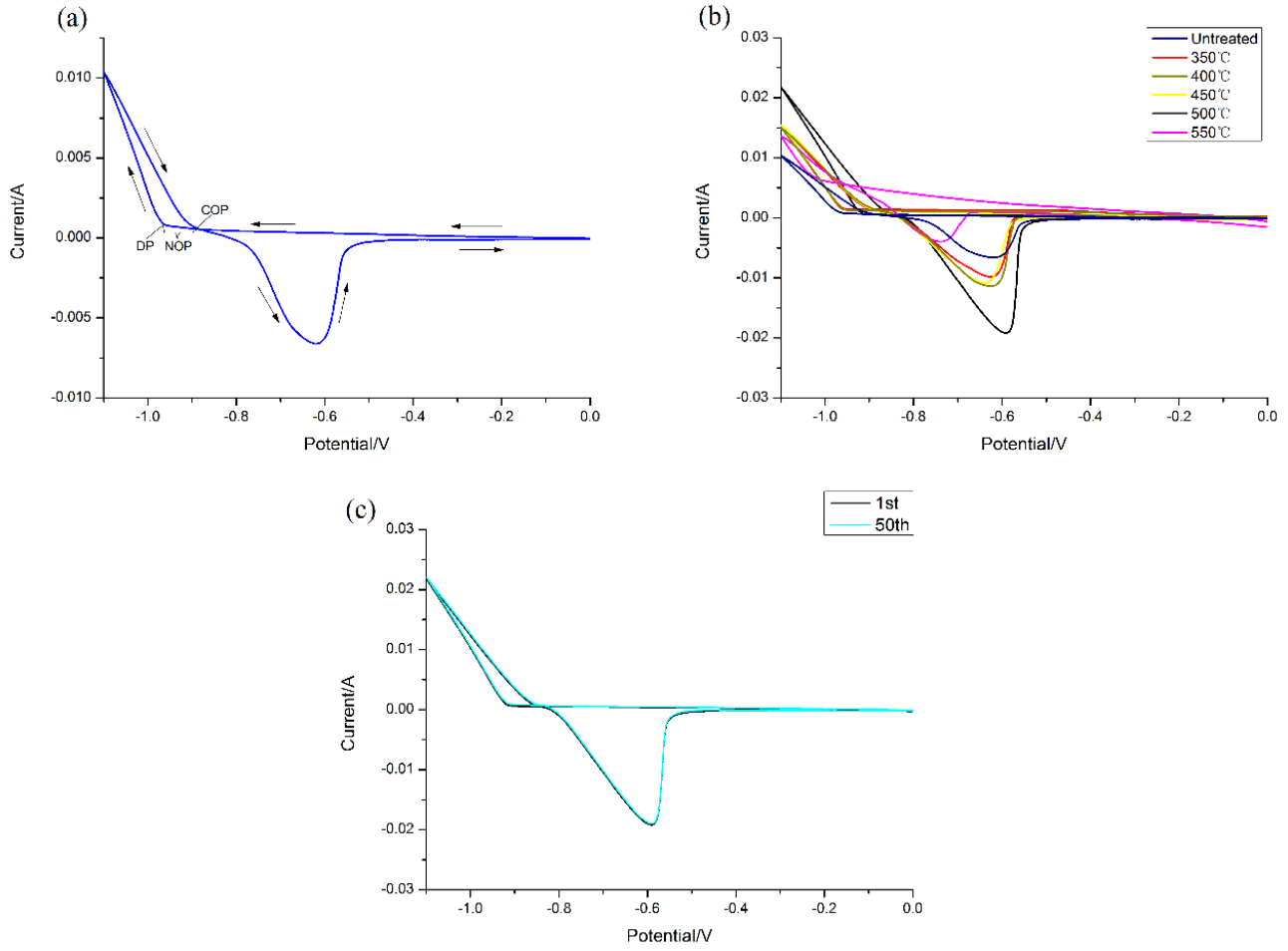

Figure 1. CV results. (a) CV plots of zinc deposition on CF surface, (b) Comparisons of CF and pyrolytic CFs at different temperatures, (c) 50 cycles of CF-500 °C at a scan rate of 10 mV s^{-1}.

The electrochemical properties of CFs were further investigated by EIS. Fig. 2 depicts the Nyquist plots of six different electrodes, all of which consist of a high frequency semicircles and a low frequency linear part. The diameter of the semicircle represents the charge transfer resistance (R_{ct}), and the linearity is partly attributed to the mass diffusion process [35-37]. The results show that the diameter of the pyrolytic CFs are smaller than that of the untreated one, confirming that the Zn^{2+}/Zn charge transfer resistance is reduced on the CF surface after pyrolytic. This may be due to the increase The increase in graphitization degree and surface area, which enhance the electrochemical catalytic activity of Zn^{2+}/Zn redox reaction [30]. The charge transfer resistance of CFs decreases as the temperature of the pyrolytic increases. However, there is a slight increase in the transfer resistance at CF-550 °C compared to CF-500 °C, which is in agreement with the CV results. This again confirms that the thermal oxidation temperature is a very important factor that affects the deposition performance.

Table 1. CV comparing the electrochemical performance of CFs

	DP (mV)	COP (mV)	NOP (mV)	Oxidation peak potential (mV)	Oxidation peak current (mA)	Deposition current (*E*=-1.1V) (mA)
Untreated	-973	-885	88	-617	-6.6	10.3
CF-350°C	-963	-889	74	-624	-9.8	14.7
CF-400°C	-962	-891	71	-622	-11.4	15.0
CF-450°C	-962	-896	66	-635	-10.8	15.2
CF-500°C	-912	-853	59	-590	-19.2	21.8
CF-550°C	-1003	-955	76	-739	-3.9	13.5

From the results discussed above, CF-500 °C has the best deposition performance. Therefore we focused on CF-500 °C for research and discussion. Fig. 3a presents the XRD spectra of original CF and CF-500 °C comparisons. Two significant diffraction peaks at 26° and 43° were observed, corresponding to the (002) and (100) crystal planes of graphite carbon [38]. However, the untreated CF diffraction peak is the shape of the skull, which corresponds to the structure of amorphous carbon [39]. Obviously, the intensity of CF-500 °C is much stronger than that of the untreated one, and the diffraction peak is sharper, which confirms that the degree of graphitization of the carbon felt is improved by calcination, and the disordered structure is reduced. As showed in the Raman spectrum of Fig. 3b, two characteristic peaks were observed in the original CF and GF-500 °C around 1353 cm^{-1} and 1590 cm^{-1}, which are called D-band and G-band, respectively. The D-band is a characteristic state

of a disordered state or a defect state in which graphite crystal particles are decreased, and the intensity of the peak is a measure of the number of amorphous activated carbon atoms [40].

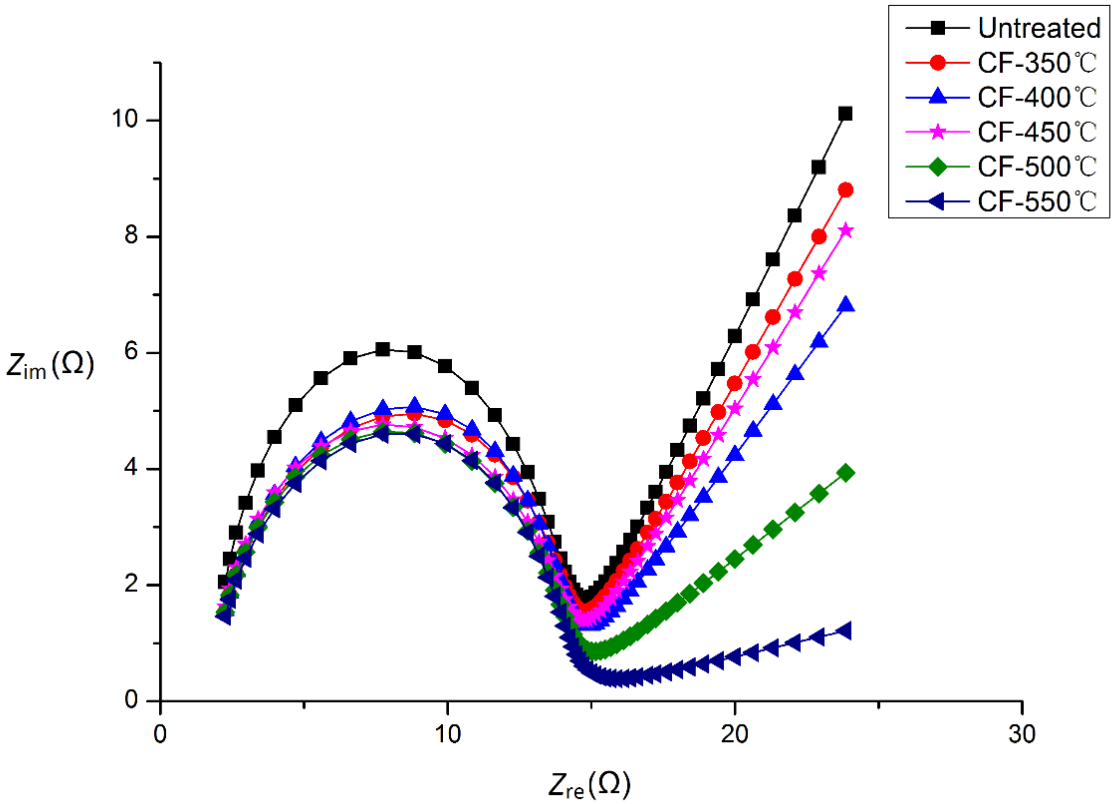

Figure 2. Nyquist plots of the different CF electrodes at deposition potentials.

And the G-band is a characteristic peak of the sp^2 structure of the graphite crystal, and its intensity can be utilized to characterize the integrity of the sp^2 hybrid bond structure in the graphite structure [40]. The D-band and G-band of the original CF are relatively weak, and the half-height width of the G-band at GF-500 °C was reduced, which means that the grain size of the carbon fiber is gradually increased, and the degree of ordering is also improved. In addition, the intensity ratio of D to G band (I_D/I_G) is refers to the crystallinity of the carbon material. After pyrolysis, the value of I_D/I_G decreased from 0.90 to 0.80, further verifying the reduction of defect structure and disorder. Moreover, the peak height of the G-band is further increased and sharper, indicating that the structure of the carbon fiber has changed, gradually changing from a two-dimensional disordered structure to a three-dimensional ordered structure. This ordered structure provides a place for uniform distribution of electrode current density, preventing electrode polarization, and promotes homogeneous deposition of zinc.

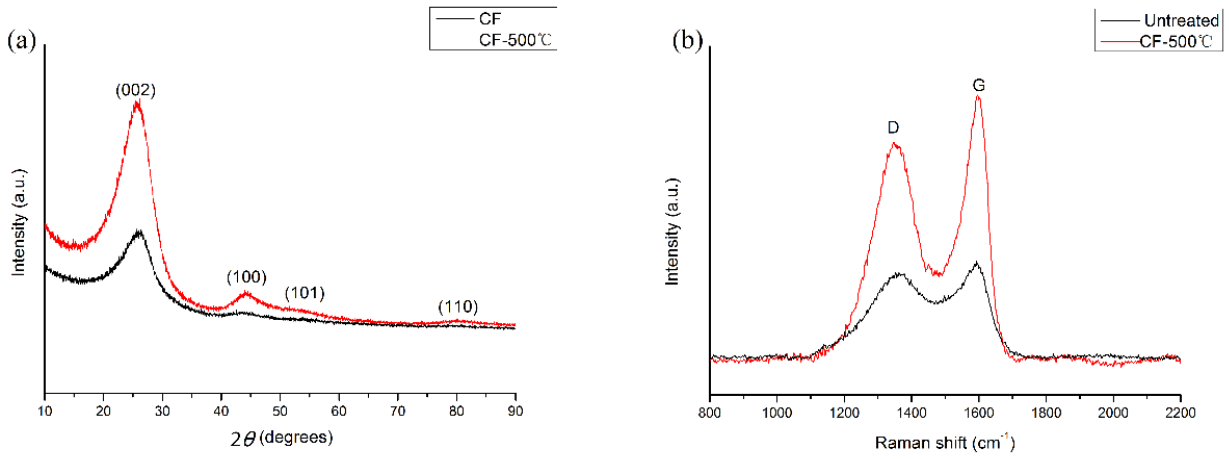

Figure 3. (a) XRD patterns and (b) Raman patterns of Original CF and CF-500 °C.

SEM images of CF and CF-500 °C are depicted in Fig. 4a-b. It can be seen that the texture on the surface of the original CF is relatively clear, and some defects such as fine etching and grooves can be observed. These grooves are due primarily to the fact that the polyacrylonitrile carbon fiber is wet-spun during the formation of the precursor [41]. In addition, white particulate impurities are present on the original CF surface, which remain in the CF production process. The main component of these impurities is some inorganic substances, which directly affect the purity of carbon fibers and the surface area implicated in electron conduction, thereby affecting their conductivity. On the surface of CF-500 °C, there are almost no impurities, and defects such as grooves, which confirmed that the a suitable pyrolysis increased the degree of graphitization of CF to make the CF surface smooth, which is consistent with the results of XRD and Raman. Fig. 4c-f reveal comparisons of zinc deposition morphology after charging process of the original CF and CF-500 °C negative electrode. See Fig. 4c, severe zinc dendrites formed on the surface of the original CF, while the zinc deposit on the surface of CF-500 °C is uniform, the particle size is small, and no zinc dendrite is formed (Fig. 4d). Fig. 4e-f shows the difference in the morphology of the original CF and CF-500 °C zinc deposits from a larger scale. The original CF surface is covered with zinc dendrites, the carbon fibers are exposed, and the deposition quality is poor, some areas are densely deposited, and some areas are sparse (Fig. 4e).

In contrast, the deposited layer on the surface of CF-500 °C is evenly compacted, the carbon fiber is not exposed, and the deposition quality is better, almost no zinc dendrite is formed, and the amount of zinc loaded is much larger than that of the original CF (Fig. 4f). These experimental results further confirmed that CF-500 °C effectively inhibited the formation of zinc dendrites during charging. On the one hand, pyrolysis enhances the degree of graphitization of the CF electrode and increases conductivity and wettability. On the other hand, the order and uniformity of the porous electrode are improved, the depolarization ability of the electrode is improved and the exchange current density can be uniformly distributed [42], thereby promoting uniform deposition and suppressing zinc dendrite.

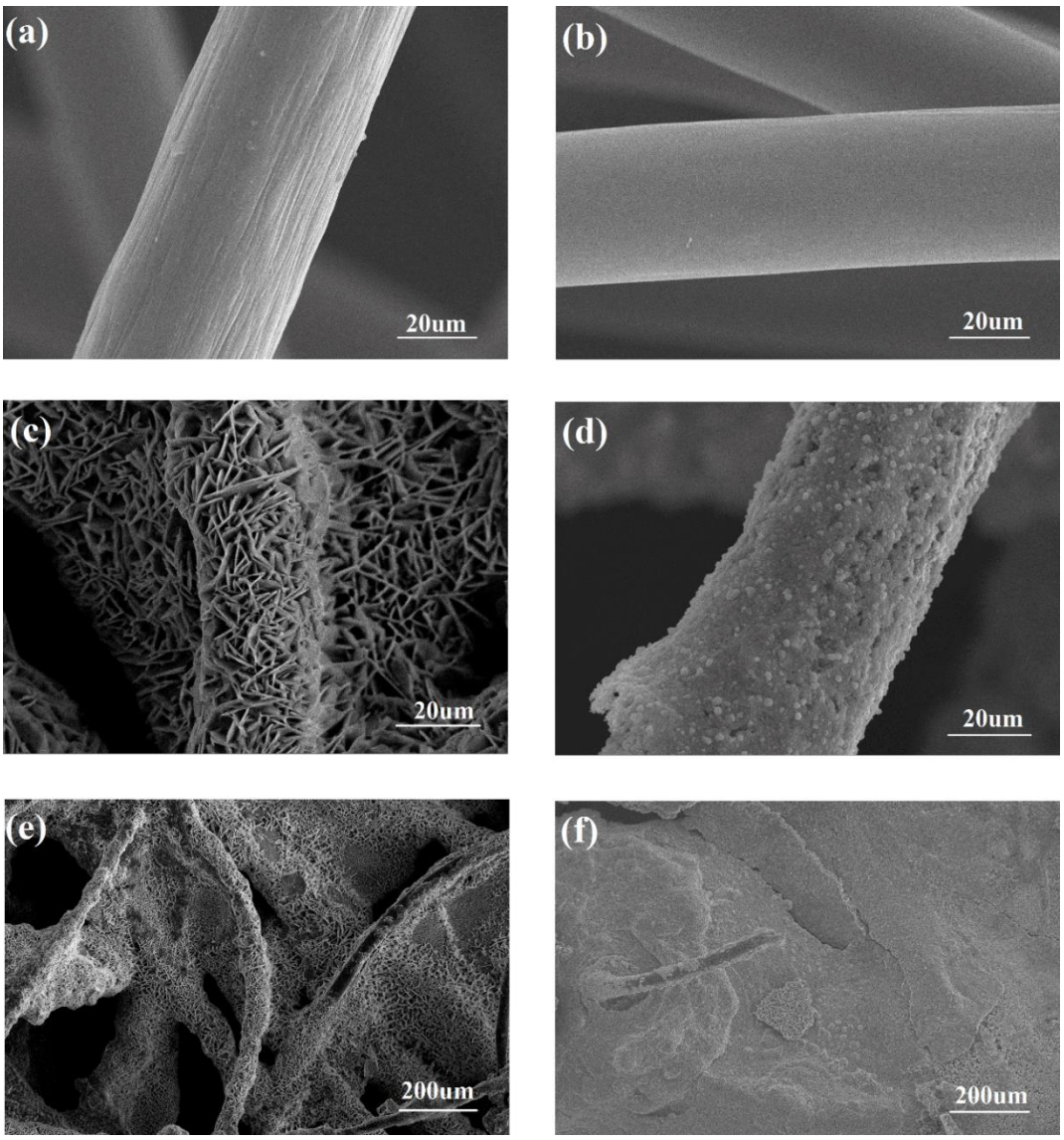

Figure 4. SEM images of (a-e) Original CF and (b-f) CF-500 °C. The (a) and (b) negative electrodes before charge process, and the (c, e) and (d, f) negative electrodes after charge process.

The practical application of CF and CF-500 °C as a negative electrode were evaluated in a laboratory scale ZBFB. The charge discharge curves recorded at a current density of 40 mA cm^{-2} were compared as showed in Fig. 5a. All batteries were charged for 30 min and then discharged. The average charging voltages of the original CF and CF-500 °C are 1.98 V and 1.94 V, respectively; and the average discharge voltages are about 1.55 V and 1.60 V. The decrease in the charging voltage and the increase in the discharge voltage are mainly attributed to the decrease in the overpotential of the negative electrode, which is that the pyrolysis reduces the electrode polarization. The original CF discharge time was only 25 min, while the CF-500 °C was close to 30 min. This is due to the loading of zinc on the CF-500 °C surface is more than CF during charging, and the discharge is a process of consuming zinc deposits. Moreover, since the zinc deposition on the surface of CF-500 °C is uniform, the discharge voltage is relatively stable. Therefore, the performance of ZBFB using CF-500 °C as a negative electrode has been greatly improved. The coulombic efficiency has increased from 91.8% to

99.3%, the voltage efficiency has increased by 82.5% from 78.2%, and the energy efficiency has reached 81.9% (Fig. 5b), which is much higher than these reported values [33, 35, 43-45]. To further reveal the rate performance of ZBFB using CF-500 °C, the battery was subjected to charge-discharge at various current densities of 20 to 80 mA cm^{-2}. As can be observed in Fig. 5c, when the current density is increased, the average charging voltage increases and the discharge voltage decreases, which is attributed to electrode polarization [46-47]. Specifically, the average charge voltage raised from 1.87 V to 2.09 V and the averaged discharge voltage dropped from 1.64 V to 1.53 V when the current density increases from 20 to 80 mA cm^{-2}. As a result, VE dropped from 87.7% to 73.2%. Moreover, the discharge time also dropped from nearly 30 min to 25 min, and the coulombic efficiency dropped from 99.8% to 95.3% as shown in Fig. 5d. This is because the high current density consumes zinc deposited faster than the low current density. Thereby reducing the discharge time, resulting in a decrease in coulombic efficiency. But even so, the energy efficiency of ZBFB using CF-500 °C with a current density of 80 mA cm^{-2} is still as high as 69.8%, and equivalent to the performance of ZBFB using CF at a current density of 40 mA cm^{-2}, which is close to the highest reported in the literature [34], further indicating that GF-500 °C has excellent depolarization capability.

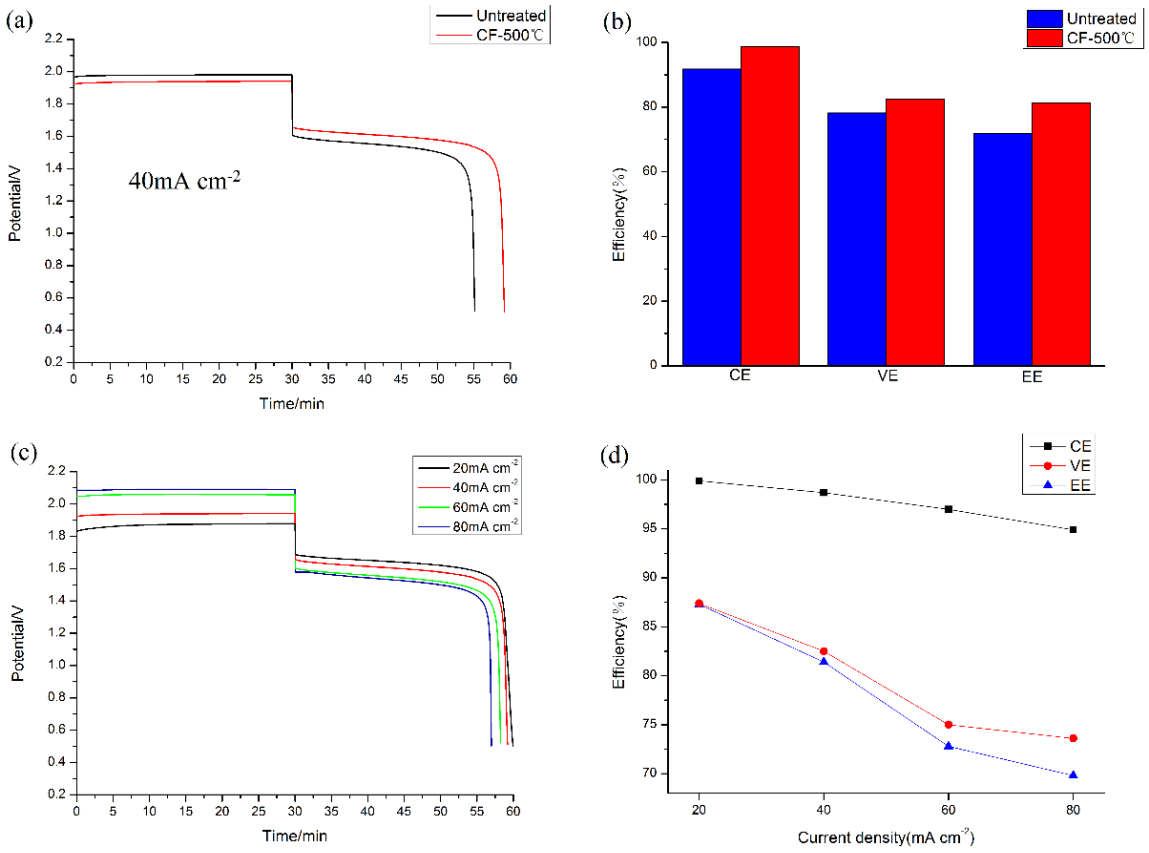

Figure 5. (a) Charge-discharge curves and (b) CE, VE and EE at a current density of 40 mA cm^{-2} of original CF and CF-500 °C, (c) Charge-discharge curves and (d) CE, VE and EE at various current densities of CF-500 °C.

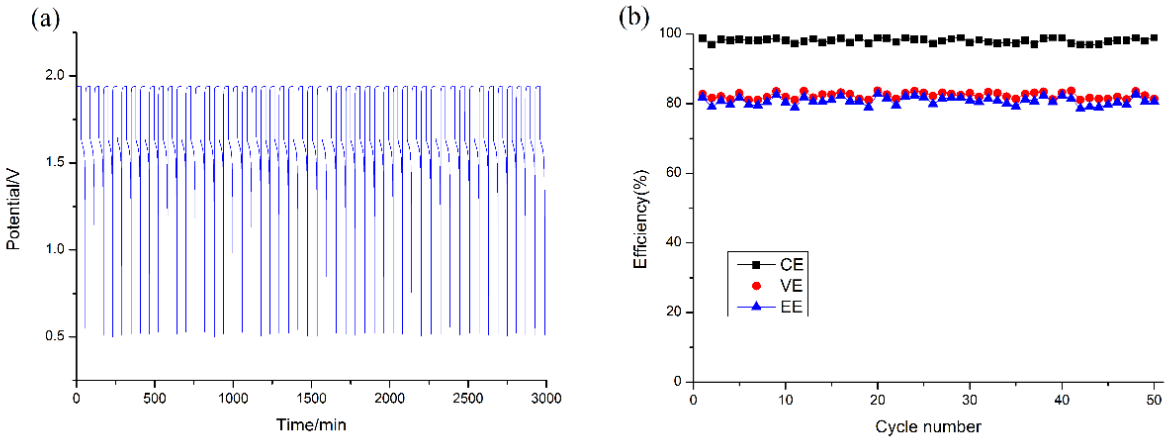

Figure 6. (a) Cycling performance of a ZBFB with CF-500 °C electrode and (b) CE, VE and EE during the 50 charge-discharge cycles.

Cyclic performance was also performed to test the stability of the GF-500 °C electrode. From the voltage versus time plot in Fig. 6a, we can see that the charging voltage remains sufficiently stable, and the discharge voltage slightly floats in the cycle, but it is negligible. In general, the entire charge-discharge curve remains in a stable state. See Fig. 5b, the overall coulombic efficiency remained above 98.6%, suggesting that there was no self-discharge caused by zinc dendrite puncturing the membrane during cyclic performance. Voltage efficiency and energy efficiency, although slightly fluctuating, they are still remained above 82% and 80%, respectively. The above experimental results show that the zinc bromine flow battery system with GF-500 °C as the negative electrode has excellent dendrite resistance and battery performance.

4. CONCLUSIONS

Pyrolytic treatment of the carbon felt can improve the order structure of the carbon felt, and fundamentally improved the depolarization ability of CF, thereby enhancing the uniform deposition of zinc. In particular, the pyrolytic carbon felt calcined at 500 °C promoted the reaction kinetics of Zn^{2+}/Zn. From SEM images, we can find that it can effectively inhibit the formation of zinc dendrites as the negative electrode of the zinc-bromine flow battery. Not only that, the coulombic efficiency reached 99.3% and the energy efficiency was as high as 82.5% at a current density of 40 mA cm^{-2}, compared with coulombic and energy efficiency of 91.8% and 71.2% with original carbon felt electrode at the same current density. Furthermore, it was demonstrated that even if ZBFB with CF-500 °C electrode operated at a high current density of up to 80 mA cm^{-2}, the energy efficiency is still as high as 69.8%, shows an excellent depolarization capability. In addition, cyclic performance also exhibits good stability, suggesting that CF-500 °C electrode not only inhibits the formation of zinc dendrites, but also improves the performance of the battery.

ACKNOWLEDGMENTS

We greatly appreciate financial support from Jilin Province Science and Technology Development Planning (Project 20170203001SF).

References

1. M. F. Akorede, H. Hizam, E. Pouresmaeil, *Renewable Sustainable Energy Rev.,* 14 (2010) 724.
2. Z. Yang, J. Zhang, M. C. Kintnermeyer, X. Lu, D. Choi, J. P. Lemmon, J. Liu, *Chem. Rev.,* 111 (2011) 3577.
3. J. P. Barton, D. G. Infield, *IEEE Trans. Power Appar. Syst.,* 19 (2004) 441.
4. B. Dunn, J. M. Tarascon, *Science,* 334 (2011), 928.
5. C. P. D. León, A. Frías-Ferrer, J. González-García, D. A. Szánto, F. C. Walsh, *J. Power Sources,* 160 (2006) 716.
6. W. Wang, Q. Luo, B. Li, X. Wei, L. Li, Z. Yang, *Adv. Funct. Mater.,* 23 (2013) 970.
7. P. Zhao, H. Zhang, H. Zhou, J. Chen, S. Gao, B. Yi, *J. Power Sources,* 162 (2006) 1416.
8. W. H. Wang, X. D. Wang, *Electrochim. Acta,* 52 (2007) 6755.
9. X. L. Zhou, T. S. Zhao, L. An, Y. K. Zeng, X. B. Zhu, *Appl. Energy,* 180(2016) 353.
10. G. Codina, A. Aldaz, *J. Appl. Electrochem.,* 22 (1992), 668.
11. M. Lopez-Atalaya, G. Codina, J. R. Perez, J. L. Vazquez, A. Aldaz, *J. Power Sources,* 39 (1992) 147.
12. H. Zhang, Y. Tan, J. Li, B. Xue, H. Zhang, Y. Tan, J. Li, B. Xue, *Electrochim. Acta,* 248 (2017) 203.
13. P. Zhao, H. Zhang, H. Zhou, B. Yi, *Electrochim. Acta,* 51 (2006) 1091.
14. H. S. Lim, A. M. Lackner, R. C. Knechtli, *J. Electrochem. Soc.,* 124 (1977) 1154.
15. K. Cedzynska, *Electrochim. Acta,* 40 (1995) 971.
16. J. D. Jeon, H. S. Yang, J. Shim, H. S. Kim, J. H. Yang, *Electrochim. Acta,* 127 (2014) 397.
17. C. P. D. León, F. C. Walsh, *Encyclopedia of Electrochemical Power Sources,* 1 (2009) 487.
18. M. Skyllas-Kazacos, *J. Power Sources,* 124 (2003) 299.
19. B. R. Chalamala, T. Soundappan, G. R. Fisher, M. R. Anstey, V. V. Viswanathan, M. L. Perry, *Proc. IEEE,* 102 (2014) 976.
20. N. C. Hoyt, K. L. Hawthorne, R. F. Savinell, J. S. Wainright, *J. Electrochem. Soc.,* 163 (2016) A5041.
21. K. L. Hawthorne, J. S. Wainright, R. F. Savinell, *J. Power Sources,* 269 (2014), 216.
22. W. H. Mulder, J. H. Sluyters, T. Pajkossy, L. Nyikos, *J. Electroanal. Chem.,* 285 (1990) 103.
23. J. Robertson, *Curr. Opin. Solid State Mater. Sci.,* 1 (1996) 317.
24. Z. González, A. Sánchez, C. Blanco, M. Granda, R. Menéndez, R. Santamaría, *Electrochem. Commun.,* 13 (2011) 1379.
25. B. Li, M. Gu, Z. Nie, Y. Shao, Q. Luo, X. Wei, X. Li, J. Xiao, C. Wang, V. Sprenkle, *Nano Lett.,* 13 (2013) 1330.
26. X. Wu, H. Xu, P. Xu, Y. Shen, L. Lu, J. Shi, J. Fu, H. Zhao, *J. Power Sources,* 263 (2014) 104.
27. M. Wu, T. Zhao, R. Zhang, H. Jiang, L. Wei, *Energy Technology,* 6(2018) 333.
28. W. H. Wang, X. D. Wang, *Electrochim. Acta,* 52 (2007) 6755.
29. T. J. Rabbow, M. Trampert, P. Pokorny, P. Binder, A. H. Whitehead, *Electrochim. Acta,* 173 (2015) 17.
30. P. Mazúr, J. Mrlík, J. Beneš, J. Pocedič, J. Vrána, J. Dundálek, J. Kosek, *J. Power Sources,* 380 (2018) 105.
31. B. Sun, M. Skyllas-Kazacos, *Electrochim. Acta,* 37 (1992) 1253.
32. S. Fletcher, *Electrochim. Acta,* 28 (1983) 917.
33. X. Sun, T. Souier, M. Chiesa, A. Vassallo, *Electrochim. Acta,* 148 (2014) 104.

34. M. C. Wu, T. S. Zhao, H. R. Jiang, Y. K. Zeng, Y. X. Ren, *J. Power Sources,* 355 (2017) 62.
35. C. Wang, X. Li, X. Xi, P. Xu, Q. Lai, H. Zhang, *RSC Adv.,* 6 (2016) 40169.
36. F. Mansfeld, *Electrochim. Acta,* 35 (1990) 1533.
37. M. Wu, M. Liu, G. Long, K. Wan, Z. Liang, T. S. Zhao, *Appl. Energy,* 136 (2014) 576.
38. Z. H. Zhang, T. S. Zhao, B. F. Bai, L. Zeng, L. Wei, *Electrochim. Acta,* 248 (2017) 197.
39. X. C. Xiao, W. H. Jiang, L. X. Song, J. F. Tian, X. F. Hu, *Diamond Relat. Mater.,* 9 (2000) 1782.
40. A. C. Ferrari, D. M. Basko, *Nat. Nanotechnol.,* 8 (2013) 235.
41. H. O. Pierson, D. A. Northrop, *J. Compos. Mater.,* 9 (1975) 118.
42. H. R. Jiang, M. C. Wu, Y. X. Ren, W. Shyy, T. S. Zhao, *Appl. Energy,* 213 (2018) 366.
43. L. Zhang, H. Zhang, Q. Lai, X. Li, Y. Cheng, *J. Power Sources,* 227 (2013) 41.
44. G. P. Rajarathnam, M. E. Easton, M. Schneider, A. F. Masters, T. Maschmeyer, A. M. Vassallo, *RSC Adv.,* 6 (2016) 27788.
45. M. Schneider, G. P. Rajarathnam, M. E. Easton, A. F. Masters, T. Maschmeyer, A. M. Vassallo, *RSC Adv.,* 6 (2016) 110548.
46. Q. Lai, H. Zhang, X. Li, L. Zhang, Y. Cheng, *J. Power Sources,* 235 (2013) 1.
47. Y. Munaiah, S. Dheenadayalan, P. Ragupathy, V. K. Pillai, *ECS J. Solid State Sci. Technol.,* 2 (2013) M3182-M3186.